

Transverse instability and disintegration of domain wall of relative phase in coherently coupled two-component Bose-Einstein condensates

Kousuke Ihara and Kenichi Kasamatsu

Department of Physics, Kindai University, Higashi-Osaka, Osaka 577-8502, Japan

(Dated: February 26, 2022)

We study transverse instability and disintegration dynamics of a domain wall of a relative phase in two-component Bose-Einstein condensates with a coherent Rabi coupling. We obtain analytically the stability phase diagram of the stationary solution of the domain wall for the one-dimensional coupled Gross-Pitaevskii equations in the plane of the Rabi frequency and the intercomponent coupling constant. Outside the stable region, the domain wall is dynamically unstable for the transverse modulation along the direction perpendicular to the phase kink. The nonlinear evolution associated with the instability is demonstrated through numerical simulations for both the domain wall without edges and that with edges formed by the quantized vortices.

PACS numbers: 03.75.Kk 03.75.Lm

I. INTRODUCTION

Solitons in multidimensional systems are generally unstable, known as the transverse instability [1, 2], where the solitonic structure is dynamically unstable against the symmetry-breaking modulation along the unbounded spatial dimension. Bose-Einstein condensates (BECs) are well-suited system to study such an unstable properties of solitons. This is because: (i) The properties of BECs are described by the Gross-Pitaevskii (GP) (non-linear Schrödinger) equation, which allows various solitary wave solutions. (ii) The system consists of dilute gases and is almost far from dissipation so that nonequilibrium processes of unstable dynamics can be directly observed from the well-defined initial states. (iii) The topological solitons can be created by well-developed phase-engineering techniques. Given all three of these advantages, dynamical instabilities of solitons have indeed been observed in dilute BECs. For example, the dark solitons in two-dimensional (2D) BECs are broken up to an array of vortex pairs due to the transverse instability, called “snake instability” [3, 4]. The decay of a planar dark soliton into a vortex ring was observed experimentally in a 3D BEC [5, 6].

For two-component BECs described by the two-component order parameters, the structures of solitons are richer than those in single-component BECs, e.g., dark solitons [7], dark-bright solitons [8, 9], domain walls [10], and magnetic solitons [11]. For a typical two-component mixture of BECs, the U(1) phases in each component are independent variables, because the two components are coupled only through the density-density coupling. However, when a Rabi coupling is applied between the internal states of two-component BECs, the symmetry associated with one of the two U(1) phases is broken, and the relative phase between the two components makes sense. Then, the new type of soliton can exist as “a domain wall of the relative phase” which is obtained as a kink solution of the sine-Gordon equation for the two-component BECs [12]. This domain wall can exist as a bound string between two vortices in two-

component BECs, which results in a molecule of the vortices [13].

Recently, real time dynamics of the aforementioned vortex molecule in the Rabi-coupled condensates have been studied by some authors [14–16]. The authors in Refs.[14, 16] have especially stressed that this system can be used as the analogous simulations of the “confinement” in quark–anti-quark phenomena. Tylutki *et al.* studied the precession dynamics of the vortex molecule as a function of the Rabi coupling and the molecular distance [14]. In a certain regime, the domain wall was found to disintegrate into some parts, which is analogous to the string breaking phenomena in quantum chromodynamics. This observation was further confirmed by the simulations by Eto and Nitta [16].

Here, we reveal the physical origin of this disintegration as the instability associated with the transverse displacement of the domain wall, i.e, the snake instability. We obtain an exact solution of the domain wall for the 1D coupled GP equations for two-component BECs, making a phase diagram of the stationary solutions in the plane of the intercomponent coupling strength and the Rabi frequency. The energetic stability of the solution reproduces the previous work by Usui and Takeuchi [17]. In the unstable regime, the dynamical instability takes place for the transverse modulation along the direction perpendicular to the sine-Gordon kink, which is analyzed by the Bogoliubov-de Gennes (BdG) equation. The nonlinear dynamics associated with this instability are shown by direct numerical simulations of the 2D GP equation for the domain wall without edges and with edges formed by quantized vortices. The disintegration observed in previous works [14, 16] can be explained as the manifestation of the snake instability.

The paper is organized as follows. After introducing the formulation of the problem in Sec. II, we first study the stability of the domain wall of the relative phase based on the exact solution of the GP equation in Sec. III A. Next, the transverse instability of the domain wall is discussed through the BdG analysis in Sec. III B. In Sec. IV we demonstrate the dynamics due to the trans-

verse instability using the direct numerical simulations of the 2D GP equations. Section V is devoted to the conclusion.

II. FORMULATION

We consider two-component BECs of ultracold atoms having the same mass m and residing in two different hyperfine states. The BECs are described by the condensate wave functions Ψ_j ($j = 1, 2$). The equilibrium state of the system is obtained by minimizing the Gross-Pitaevskii (GP) energy functional

$$E[\Psi_1, \Psi_2] = \int d\mathbf{r} \left[\sum_{j=1,2} \left(\Psi_j^* h \Psi_j + \frac{g_j}{2} |\Psi_j|^4 \right) + g_{12} |\Psi_1|^2 |\Psi_2|^2 - \frac{\hbar \Omega_R}{2} (\Psi_1^* \Psi_2 + \Psi_1 \Psi_2^*) \right]. \quad (1)$$

Here, $h = -\hbar^2 \nabla^2 / (2m) + V_{\text{ext}}$ is the single-particle Hamiltonian with the trapping potential V_{ext} . The coupling constants g_j ($j = 1, 2$) and g_{12} represent the strength of intra- and the intercomponent interactions, respectively, described as $g_j = 4\pi \hbar^2 a_j / m$ and $g_{12} = 4\pi \hbar^2 a_{12} / m$ with the s -wave scattering lengths a_i and a_{12} between the corresponding atoms. We assume that the intracomponent coupling constants satisfy $g_1 = g_2 = g > 0$ for simplicity. The last term in Eq. (1) describes a coherent Rabi coupling induced by an external electromagnetic field, which allows atoms to transfer their internal states coherently [18, 19]; Ω_R stands for the Rabi frequency. Then, the total number $N = N_1 + N_2 = \int d\mathbf{r} (|\Psi_1|^2 + |\Psi_2|^2)$ is a constant of motion. In the following analysis except the numerical simulations in Sec. IV B, we assume the homogeneous system by setting $V_{\text{ext}} = 0$. For the coupling constants, we confine ourselves to the range $-1 < g_{12}/g < 1$ corresponding to a miscible regime without the Rabi coupling, otherwise the components phase separate for $g_{12} > g$ [20, 21] or undergo mean-field collapse for $g_{12} < -g$ [22]. The properties of a domain wall of the condensate densities for $g_{12} > g$ in the presence of the Rabi-coupling have been studied in detail in Ref. [23].

The time-dependent GP equations are given by the variational procedure $i\hbar \partial \Psi_j / \partial t = \delta E / \delta \Psi_j^*$ as

$$i\hbar \frac{\partial \Psi_1}{\partial t} = -\frac{\hbar^2 \nabla^2}{2m} \Psi_1 + g |\Psi_1|^2 \Psi_1 + g_{12} |\Psi_2|^2 \Psi_1 - \frac{\hbar \Omega_R}{2} \Psi_2, \quad (2)$$

$$i\hbar \frac{\partial \Psi_2}{\partial t} = -\frac{\hbar^2 \nabla^2}{2m} \Psi_2 + g |\Psi_2|^2 \Psi_2 + g_{12} |\Psi_1|^2 \Psi_2 - \frac{\hbar \Omega_R}{2} \Psi_1. \quad (3)$$

First, we consider the ground state in the homogeneous system by ignoring the time and spatial derivative terms in Eqs. (2) and (3). Because of the conservation of the total particle number, the chemical potential as a Lagrange multiplier for both components should be common as $\mu_1 = \mu_2 = \mu$, the stationary wave function being

written as $\Psi_j = \sqrt{n_j} e^{i\theta_j - i\mu t/\hbar}$. Then, the relative phase $\theta = \theta_1 - \theta_2$ should be vanished, because the energy of the Rabi-coupling term $-\hbar \Omega_R \sqrt{n_1 n_2} \cos \theta$ is minimized at $\theta = 0$. As a result, the densities in the miscible regime satisfy $n_1 = n_2 \equiv n_0$ with

$$n_0 = \frac{\mu + \hbar \Omega_R / 2}{g + g_{12}}. \quad (4)$$

The miscible regime takes place when the intercomponent coupling constant satisfies $g_{12} < g + \hbar \Omega_R / (n_1 + n_2)$ [24], otherwise the equilibrium state involves spontaneous density imbalance.

We scale the wave function as $\Psi_j = \sqrt{n_0} \psi_j$, and introduce the length, time, and energy scale as $\xi = \hbar / \sqrt{2mg n_0}$, $\hbar / (g n_0)$, and $g n_0$, respectively. Then, we get the dimensionless GP equation,

$$i \frac{\partial \psi_1}{\partial t} = -\nabla^2 \psi_1 - \tilde{\mu} \psi_1 + |\psi_1|^2 \psi_1 + \gamma |\psi_2|^2 \psi_1 - \omega_R \psi_2, \quad (5)$$

$$i \frac{\partial \psi_2}{\partial t} = -\nabla^2 \psi_2 - \tilde{\mu} \psi_2 + |\psi_2|^2 \psi_2 + \gamma |\psi_1|^2 \psi_2 - \omega_R \psi_1. \quad (6)$$

Here, all the variables are dimensionless and the coefficients are given as

$$\omega_R = \frac{\hbar \Omega_R}{2g n_0}, \quad \gamma = \frac{g_{12}}{g}, \quad \tilde{\mu} = 1 + \gamma - \omega_R. \quad (7)$$

III. TRANSVERSE INSTABILITY OF DOMAIN WALL OF RELATIVE PHASE

In the seminal paper [12], Son and Stephanov showed that the GP equation for the Rabi-coupled two-component BECs can be reduced to the sine-Gordon equation when the gradient of the density is neglected. Considering the 1D system along the x -axis and substituting the expression $\psi_j(x) = e^{i\theta_j(x)}$ into Eqs. (5) and (6), we get the sine-Gordon equation

$$\frac{\partial^2 \theta}{\partial x^2} = 2\omega_R \sin \theta \quad (8)$$

with the relative phase $\theta \equiv \theta_1 - \theta_2$ and the constant C of integral. The stationary solution for the boundary conditions $\theta = \pi \pm \pi$ and $\partial_x \theta = 0$ for $x \rightarrow \pm \infty$ is given by

$$\theta(x) = 4 \arctan e^{\sqrt{2\omega_R} x}. \quad (9)$$

This solution is known as the sine-Gordon soliton [12]. The stability criterion was obtained as $\omega_R^c = (1 - \gamma)/3$ by neglecting the density gradient, which is valid for $\gamma \sim 1$. Son and Stephanov proposed that, when vortices are present in two-component BECs, the Rabi coupling can bind a pair of vortices in the different components via the sine-Gordon domain wall. After that the binding of

vortices and composite structures of the resulting vortex molecules have been studied in various situations [14–16, 25–32].

In this section, we consider the stability of the domain wall of the relative phase based on the GP equations (5) and (6), where we take account of the contribution of the density gradient. We first consider the energetic stability of the domain wall. Although this problem has been considered by several papers [12, 17, 33], we employ the exact solution of the domain wall and extend the phase diagram to the region of the negative intercomponent coupling $\gamma < 0$. Next, we consider the transverse instability by extending the 1D domain wall to the additional spatial dimension. The stability can be studied by the BdG analysis, where the signal of the instability is shown by the appearance of the imaginary excitation frequency of the Bogoliubov modes.

A. Exact solution and energetic instability

We consider the energetic stability of the domain wall of the relative phase by solving the 1D version of the GP equations (5) and (6). We seek the stationary solutions which satisfy $|\psi_j| = 1$ at infinity and the phases change continuously as $0 \rightarrow +(-)\pi$ for ψ_1 (ψ_2) from $x = -\infty$ to $x = +\infty$. For the sine-Gordon soliton and our symmetric parameters, the solution should satisfy the relation $\psi_1 = \psi_2^*$. This restriction reduces the equations to

$$-\frac{\partial^2 \psi_1}{\partial x^2} - \tilde{\mu} \psi_1 + (1 + \gamma)|\psi_1|^2 \psi_1 - \omega_R \psi_1^* = 0, \quad (10)$$

which allows us to get an expression of the exact solution of Eqs. (5) and (6) as

$$\begin{aligned} \psi_1 = \psi_2^* &= -\tanh(\sqrt{2\omega_R}x) + iA \operatorname{sech}(\sqrt{2\omega_R}x), \\ A &= \sqrt{\frac{1 + \gamma - 4\omega_R}{1 + \gamma}}. \end{aligned} \quad (12)$$

The typical profile of the solution is shown in Fig. 1(a) and (b). The relative phase changes 2π around the origin over the length scale $\sim (2\omega_R)^{-1/2}$. The density profile is written as $n_1 = n_2 = \tanh^2(\sqrt{2\omega_R}x) + A^2 \operatorname{sech}^2(\sqrt{2\omega_R}x)$, being uniform only for $\omega_R = 0$. With increasing ω_R , the spatial profile of θ approaches to a step function and the density depression becomes deeper. The solution of Eq. (11) is effective below the upper bound of the Rabi frequency $\omega_R^u = (1 + \gamma)/4$, at which the solution coincides with the form of the dark soliton with exactly zero density at the center. Physically, this boundary is interpreted as that the length scale $(2\omega_R)^{-1/2}$ is equal to the healing length given by the effective coupling constant $1 + \gamma$ [see Eq. (10)].

Figure 1(c) shows the phase diagram representing the energetic stability of the single domain wall in the γ - ω_R plane. Below the line $\omega_R = \omega_R^u$, we have the solution of the domain wall of Eq. (11). Here, we check numerically the energetic stability of the solution Eq. (11) through

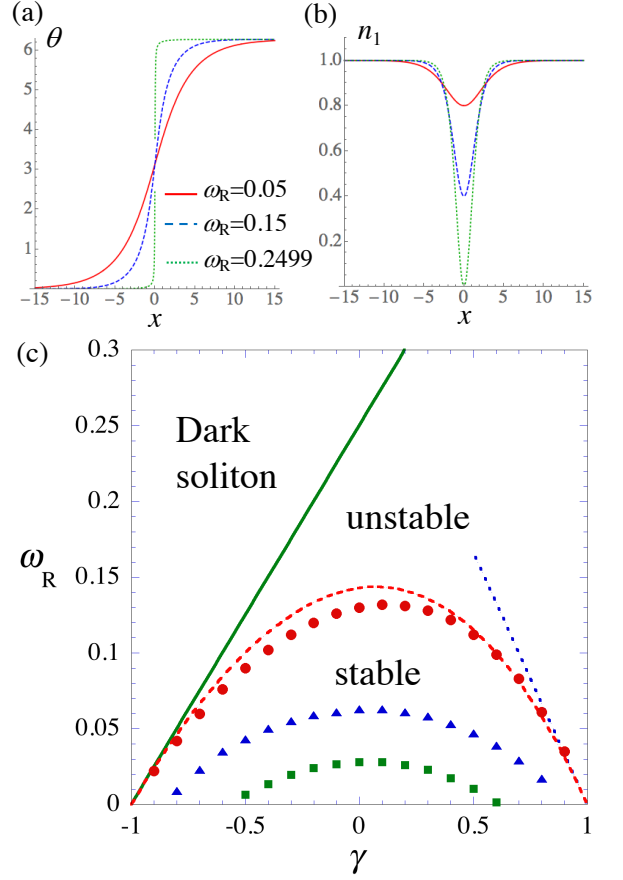


FIG. 1. The upper panels show the profile of the relative phase $\theta = \theta_1 - \theta_2$ (a) and the density $n_1 = n_2$ (b) of the exact solutions for $\gamma = 0$ and several values of ω_R . The lower panel (c) represents the phase diagram of the sine-Gordon domain wall in the γ - ω_R plane. The red filled circles represent the stability boundary obtained by the imaginary time propagation of the GP equations. The green solid line, the red dashed curve, and the blue dotted line represent $\omega_R = \omega_R^u$, $\omega_R = \omega_R^c$ by Eq. (13), and $\omega_R = \omega_R^c$ in Ref. [12], respectively. The blue triangles and green squares are stability boundary for the moving domain wall with $V = 0.2$ and $V = 0.4$, respectively, discussed in Sec. IV B.

the imaginary time propagation of the GP equations (5) and (6), which is plotted in Fig. 1(c). When the solution is unstable, the density difference grows and unwinds the 2π difference of the relative phase to zero, leading to the uniform solution [17]. The stable range of ω_R becomes narrower with increasing $|\gamma|$ and vanishes at $\gamma = \pm 1$.

This result agrees with the previous works [12, 17]. Near $\gamma \sim 1$, the plots are fitted $\omega_R^c = (1 - \gamma)/3$ obtained in [12]. Usui and Takeuchi extended the analysis by considering the density depression through the numerical and variational analyses [17]. They proposed that the instability is associated with the Landau instability of the local counterflow across the domain wall [12] and the critical velocity was estimated by using the local density at the depression. Since the instability can occur

when the wavelength of the unstable excitation is smaller than the length scale of the domain wall, they obtained the expression for the stability as

$$\omega_R^c = \frac{1}{3} n_{\min}(\omega_R^c)(1 - \gamma). \quad (13)$$

Here, $n_{\min}(\omega_R^c)$ represents the density at the density minimum for $\omega_R = \omega_R^c$, being written as $n_{\min} = (1 + \gamma - 4\omega_R^c)/(1 + \gamma)$ by using Eq. (12). This stability criterion is also shown in the dashed curve in Fig. 1, which is in good agreement with the numerical result.

B. Transverse instability of the domain wall

Next, we further study the stability of the sine-Gordon domain wall by the BdG analysis. Especially, we include

the fluctuation along the direction (y -axis) perpendicular to the sine-Gordon soliton in the x -axis to study the transverse instability.

In the standard BdG analysis, the wave function is expanded around the stationary solution ψ_j^0 as

$$\psi_j = \psi_j^0 + [u_j(x)e^{iky-i\omega t} - v_j^*(x)e^{-iky+i\omega t}]. \quad (14)$$

Here, the fluctuation along the y -direction is included by the plane wave $\propto e^{iky}$ [34, 35]. Substituting this expression into Eqs. (5) and (6), we get the eigenvalue equation. The eigenfrequency ω is calculated by solving the BdG equation

$$\hat{\mathcal{H}}\mathbf{u} = \hbar\omega\mathbf{u}, \quad \hat{\mathcal{H}} = \begin{pmatrix} \hat{h}_1 & -(\psi_1^0)^2 & \gamma\psi_1^0\psi_2^{0*} - \omega_R & -\gamma\psi_1^0\psi_2^0 \\ (\psi_1^{0*})^2 & -\hat{h}_1 & \gamma\psi_1^{0*}\psi_2^0 & -(\gamma\psi_1^{0*}\psi_2^0 - \omega_R) \\ \gamma\psi_1^{0*}\psi_2^0 - \omega_R & -\gamma\psi_1^0\psi_2^0 & \hat{h}_2 & -(\psi_2^0)^2 \\ \gamma\psi_1^{0*}\psi_2^{0*} & -(\gamma\psi_1^0\psi_2^{0*} - \omega_R) & (\psi_2^{0*})^2 & -\hat{h}_2 \end{pmatrix}, \quad (15)$$

where $\mathbf{u} = (u_1, v_1, u_2, v_2)^T$ and $\hat{h}_j = -\partial_x^2 + k^2 - \tilde{\mu} + 2|\psi_j^0|^2 + \gamma|\psi_j^0|^2$, where $j = 1(2)$ for $j = 2(1)$. Employing the domain wall solution for ψ_j^0 , we numerically solve Eq. (15) with the finite system size $-60 \leq x \leq 60$ and the 600 grid points. To this end, starting from Eq. (11) which is a solution in an infinite system, we make imaginary time propagation of the GP equation to get the proper solution ψ_j^0 for the finite-size system.

The eigenvalues of the BdG equation can be used to clarify the stability properties of the stationary solutions. Let us first consider the situation $k = 0$, where the only 1D perturbation is present. In the stable region in Fig. 1, there are positive eigenfrequencies and one zero-energy mode when we take only eigenmodes with positive norm $\sum_j \int dx (|u_j|^2 - |v_j|^2) > 0$. When the solution enters the unstable region in Fig. 1, there appears the negative eigenvalue, a signature of the energetic Landau instability. The magnitude of the negative eigenvalue is very small in the most of unstable region, which implies that the Landau instability is very weak. The imaginary time propagation confirms this feature, because the decay of the initial domain wall solution to the uniform one needs very long time. Thus, we expect that this instability is not significant in cold gas experiments at ultralow temperatures.

The more significant instability is the dynamical one. When we include the eigenmodes with finite k , there appear imaginary components in the excitation frequencies. Figure 2(a) shows the imaginary part of the excitation

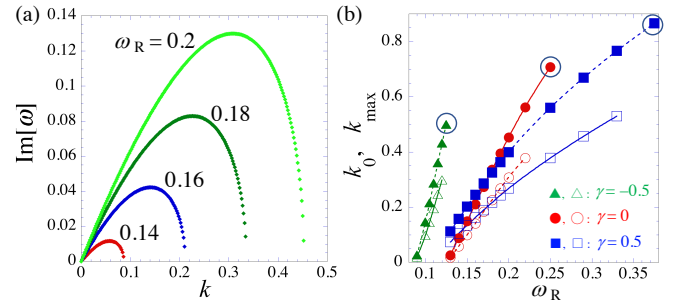


FIG. 2. The transverse instability of the domain wall solution Eq. (11). In (a), the imaginary part of the excitation frequency ω as a function of k for $\gamma = 0$ is plotted for several values of ω_R . For a given ω_R the imaginary component appears in the region $0 < k < k_{\max}$ and $\text{Im}[\omega]$ takes the maximum at $k = k_0$; we define k_0 and k_{\max} as what gives the maximum of $\text{Im}[\omega]$ and the upper bound of the unstable region, respectively. In (b), we plot k_0 (open symbols) and k_{\max} (filled symbols) as a function of ω_R for $\gamma = 0, \pm 0.5$. The curves are interpolation as a guide. The symbols enclosed by circles correspond to the values of k_{\max} for a dark soliton of a single-component condensate.

frequency as a function of k for $\gamma = 0$ and several values of ω_R . The imaginary part appears for the finite range $0 < k < k_{\max}$ and takes a maximum value at a certain wave number $k = k_0$. The unstable range of k is extended and the maximum of $\text{Im}[\omega]$ is enhanced with increasing ω_R . Thus, the instability becomes stronger with

increasing ω_R . In Fig. 2(b), we also plot k_0 and k_{\max} as a function of ω_R for $\gamma = 0, \pm 0.5$. Extrapolation of the curves to $k_0 = k_{\max} = 0$ gives the critical values ω_R^c of the dynamical stability for each γ , which agrees with the numerically obtained ω_R^c in Fig. 1. We see that the parameter region exhibiting the transverse instability coincides with the unstable region of Fig. 1. For $\omega_R > \omega_R^u$ the solution reduces to the dark soliton, where the transverse instability is expected according to the previous literature [3, 4]. As seen in Fig. 2(b), the plots are connected to the values of k_{\max} for the transverse instability of the dark soliton at $\omega_R = \omega_R^u = (1 + \gamma)/4$; we have $k_{\max} = \sqrt{(1 + \gamma)/2}$ for a dark soliton (see Eq. (7.3) in Ref. [1]) following our notation of Eq.(10).

IV. DISINTEGRATION DYNAMICS OF A DOMAIN WALL OF RELATIVE PHASE

In this section, we perform numerical simulations of the GP equations to demonstrate the disintegration of the domain wall of the relative phase through the transverse instability. We consider two cases: (i) an extended domain wall without the edges in a uniform system, and (ii) a domain wall with a finite length in a cylindrical trap. In the latter case, the edges of the wall correspond to the vortices with the same circulation in each component. The disintegration of the domain wall has been found in the numerical simulations in Refs. [14, 16], when the separation of the vortices and the Rabi frequency are large. The transverse instability of a moving domain wall without edges in trapped BECs has been reported by C. Qu *et al.* [33].

Typical structures of the domain wall corresponding to the situations (i) and (ii) are shown in Fig. 3. In the contour plots of θ , we show it within the range $-\pi \leq \theta \leq \pi$ for clarity instead of $0 \leq \theta \leq 2\pi$, where we have 2π phase jump at the center of the wall. Then, the wall can be visualized as the localized pattern as shown in Figs. 3(a) and (c), as done in the previous papers [13, 14, 16]. Figure 3 (a) shows the domain wall extended along the y -direction, which gives the initial state of the time development in Fig. 4(b).

This situation (ii) is deeply connected with the experimental observation. A straightforward way to prepare the domain wall of the relative phase in two-component BECs is that vortices are prepared in each component and then the internal states are coupled by rf fields to induce the Rabi coupling. Then, the vortices are connected with the domain wall of the relative phase. Figures 3 (c) and (d) show the typical structure of the vortex molecule. The ψ_1 -component has a vortex at $(x, y) = (0, 22.5)$ with the positive unit winding and the ψ_2 -component has a vortex at $(x, y) = (0, -22.5)$ with the same positive unit winding. When the Rabi coupling is applied, the relative phase between two components tends to become zero over the entire space. However, the phase kinks due to the vortices leave a localized structure in the relative

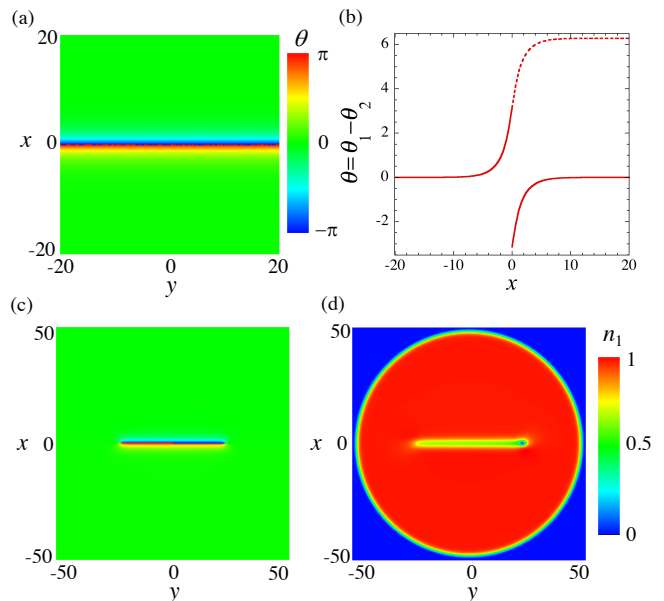


FIG. 3. The structure of the domain wall of the relative phase in a 2D space. The panels (a) and (b) associate with the situation (i) for $\gamma = 0$ and $\omega_R = 0.15$, while (c) and (d) with the situation (ii) for $\gamma = 0$, $\omega_R = 0.1$, and the length $L = 45$ in the cylindrical trap of Eq. (16). In (c) and (d), a vortex with a unit winding in ψ_1 - (ψ_2 -) component is located at $(x, y) = (0, +(-)22.5)$. These states correspond to the initial states of the simulations. (a) and (c): The 2D profile of the relative phase $\theta = \theta_1 - \theta_2$. The range of the contourplot is $-\pi \leq \theta \leq \pi$. (b): The cross section of θ in (a) along the $y = 0$ line. Here, the solid curves represent θ within the range $-\pi \leq \theta \leq \pi$. The shift of θ by 2π for $x > 0$ highlights the structure of the sine-Gordon domain wall as shown by the dashed curve, agreement with the form of Eq. (9). (d): The density profile of ψ_1 component, corresponding to (c).

phase between the two vortices, the domain wall being naturally formed.

A. domain wall in a uniform system

We first demonstrate the nonlinear dynamics associated with the transverse instability through the simulation of the 2D GP equations (5) and (6) in a uniform system. We first prepare the initial state as $\psi_j^{\text{ini}}(x, y) = \psi_j(x)$ with the solution of Eq. (11), and calculate the time development using the Crank-Nicholson method. The system size is $[-50, 50]$ in the x - y plane with numerical grids is 1000×1000 . We take the Neumann and periodic boundary condition for x - and y - direction, respectively. To initiate the dynamical instability, we add a small random noise $\sim 10^{-6}$ to the initial wave functions. We confirm that the domain wall in the stable region in Fig. 1 is certainly stable in the real time development.

Figure 4 shows the typical snapshots of the disintegration dynamics of the domain wall of the relative phase in the unstable regime for $\gamma = 0, \pm 0.5$. The snapshots

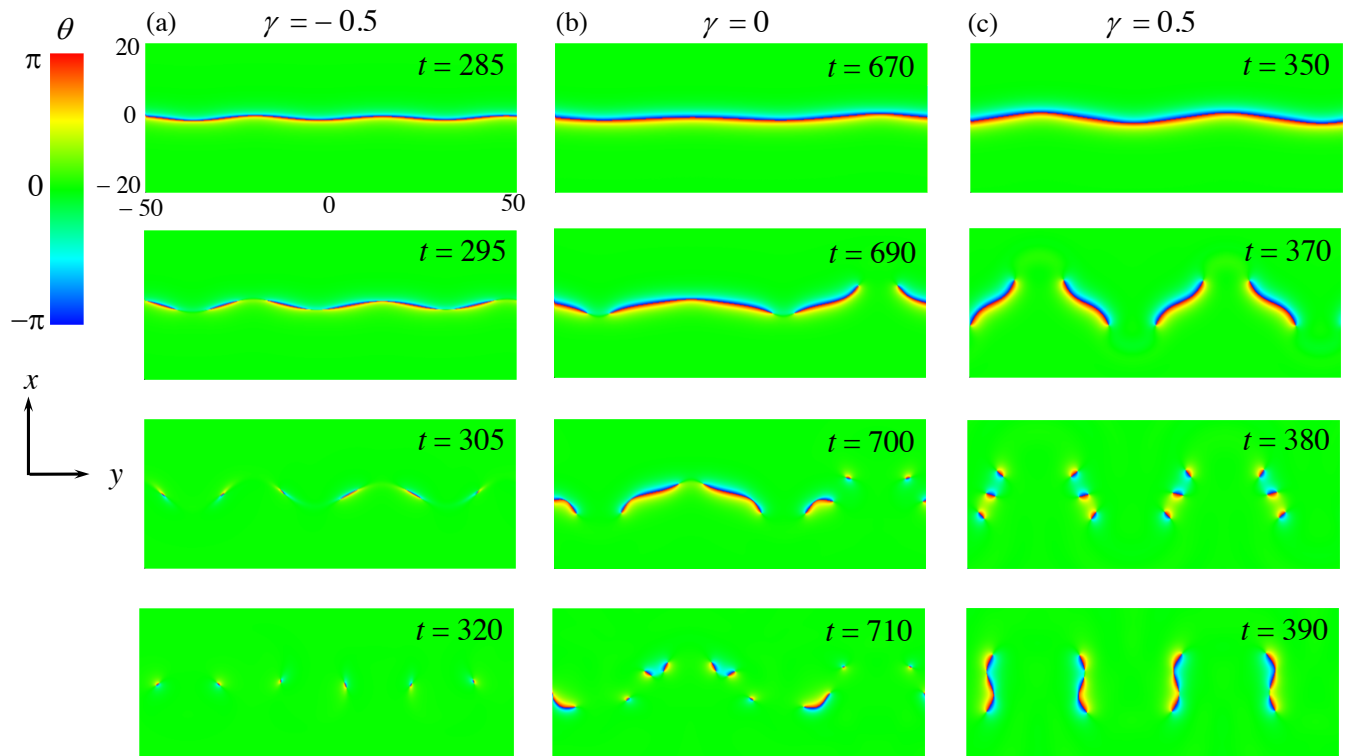


FIG. 4. The snapshot of the unstable dynamics of the domain wall of the relative phase. The panels show the profile of the relative phase defined with the range $-\pi \leq \theta \leq \pi$. The parameters are (a) $\gamma = -0.5$ and $\omega_R = 0.11$, (b) $\gamma = 0$ and $\omega_R = 0.15$, (c) $\gamma = 0.5$ and $\omega_R = 0.15$. We show the profile in the region $-20 \leq x \leq 20$ and $-50 \leq y \leq 50$.

show that the small transverse modulation of the wall is amplified after some time and leads to the disintegration of the domain wall. According to the BdG analysis, the growing time scale and the wave length of the unstable excitations are estimated as $\tau \sim 2\pi/\text{Im}[\omega(k_0)]$ and $\lambda \sim 2\pi/k_0$, respectively; for the parameters in Fig. 4, we have $(\tau, \lambda) = (114.9, 32.2)$ for (a), $(\tau, \lambda) = (247.2, 64.1)$ for (b), and $(\tau, \lambda) = (149.5, 46.5)$ for (c). The simulation results are in fairly agreement with these estimations; the quantitative deviations may be due to the finite size effect in the simulations.

After the disintegration, the dynamics of the walls exhibits different behaviors depending on γ . There, the domain wall with the finite size involves the vortices at the edges. For $\gamma = -0.5$ in Fig. 4(a), the walls rapidly shrink to zero size due to the combined attractive force by the intercomponent coupling and the Rabi coupling between the two components. In other words, the vortices at the wall edges attract each other due to the attractive vortex-vortex interaction [36] as well as the string tension caused by the Rabi coupling. For $\gamma = 0$ [Fig. 4(b)], some fragmented walls also tend to shrink due to the attraction by the Rabi coupling, but the others keep their separation. Such vortex molecules undergo center-of-mass motions, going to outside. Eventually, all the walls shrink to zero size at the later stage. Contrary to these, the subsequent dynamics for $\gamma = 0.5$ is different.

Although the initial wall disintegrates into small pieces, they keep the disintegration-merge cycle for a while, and after that some walls go to outside. In this case, the repulsive intercomponent interaction $\gamma > 0$ prevents the shrink of the wall. In equilibrium, the balance of the repulsive vortex-vortex interaction [36] and the attractive force by the Rabi coupling realizes the stable vortex molecule [13, 26, 27, 29, 32].

B. domain wall connecting vortices in a cylindrical trap

We next consider the dynamics of the domain wall having initially a finite length. This situation has been demonstrated in Refs. [14, 16]. The authors observed that the domain wall rotates due to the attractive tension between the two vortices by the Rabi coupling. However, when the separation between vortices or the Rabi coupling becomes large, the wall tends to disintegrate. Although, in general, the BdG analysis is not allowed to apply such a non-stationary configuration, we can understand qualitatively that their numerical observations are certainly due to the transverse instability as discussed below.

In simulations, we numerically solve the 2D GP equa-

tion with the cylindrical trap

$$V_{\text{ext}} = V_0 [2 + \tanh(ar - R) - \tanh(ar + R)] \quad (16)$$

with the radial coordinate r , the potential depth $V_0 = 10$ and the radius $R = 50$ of the cylinder. The sharpness of the wall boundary is represented by the parameter $a = 1$. We use the trap of Eq. (16) because there is additional contribution to the vortex dynamics from the density inhomogeneity when we employ the harmonic trap [14, 15].

We simulate the time development with the following procedure. First, the initial state without vorticity is prepared for given γ and ω_R through the imaginary time evolution of the GP equation. Next, we imprint a vortex in each component by multiplying the phase factor $e^{i\theta_v(\mathbf{r})}$ with the profile $\theta_v(\mathbf{r}) = \arctan[(y \pm y_0)/x]$ ($-$ for ψ_1 and $+$ for ψ_2) and make additional imaginary time evolution. Then, the vortex separation gradually decreases from $2y_0$, but after some time, the decreasing rate reaches a quasi-stationary behavior characterized by the slow linear decrease of the energy, which has been also reported in Ref. [16]. We stop the imaginary time evolution at a certain time in this quasi-stationary regime and use this configuration with the vortex separation $L(< 2y_0)$ as the initial state of the simulation.

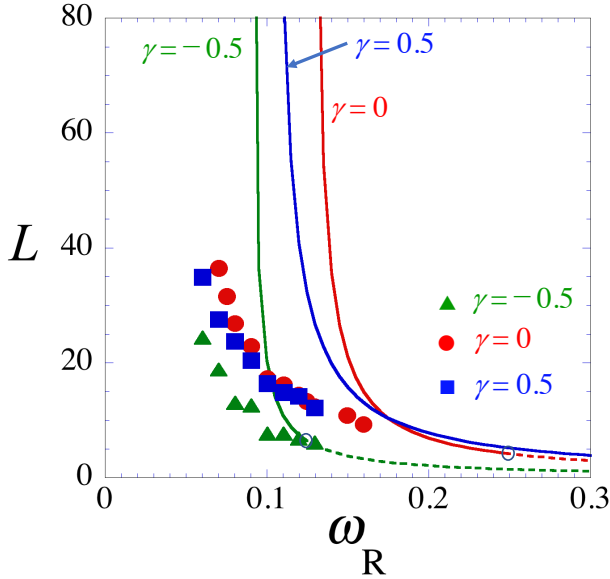


FIG. 5. The critical length for the disintegration of the domain wall with respect to the Rabi frequency ω_R . The three curves represent the estimation by the BdG analysis for $\gamma = 0, \pm 0.5$, while the plots represent the numerical results.

In this situation, we have to consider the finite size effect for the transverse instability. It is necessary for the unstable modes to grow, a half of their wave length should be smaller than the length L of the domain wall. The condition is given by $\lambda/2 = \pi/k_{\text{max}} < L$, where k_{max} can be written as a linear function of ω_R [see Fig. 2(b)]. Using this condition, we get the boundary for the disintegration of the finite-size domain wall, as depicted in

Fig. 5. With increasing the Rabi frequency ω_R , the critical length L of the wall decreases, which is consistent with the observation in Ref. [14, 16]. The stability diagram is weakly dependent on the intercomponent coupling γ .

Starting from the initial state obtained by the above procedure, we monitor the real time dynamics of the domain wall with the length L for given sets of γ and ω_R . The typical disintegration process is shown in Fig. 6 for $L = 45$, $\gamma = 0$, and $\omega_R = 0.1$. The wall initially deforms into S-shape and breaks into small pieces at the curved points. After that, the remaining wall again deforms into inverted S-shape, repeating the similar breaking process. Eventually, the wall breaks into five pieces. In this simulation, we take $\gamma = 0$ so that there is no repulsive vortex-vortex interaction. Thus, the fragmented walls eventually shrink as a result of the tension of the sine-Gordon domain wall.

When the domain wall disintegrates, the additional vortices are nucleated in each component through the snake instability. Thus, monitoring the number of vortices (phase defects) during the time developments provides a clear criterion for the disintegration; the number of vortices in each component is kept to be unity when the domain wall is stable, otherwise it is unstable. Using this criterion, we calculate the critical length of the wall as a function of ω_R for $\gamma = 0, \pm 0.5$ and plot in Fig. 5. We see that the behavior is qualitatively consistent with the BdG prediction, but quantitatively the disintegration takes place even in the region of the Rabi frequencies smaller than the critical values.

This quantitative difference may attribute to the rotation of the domain wall with the finite size [14, 16]. As mentioned before, the domain wall with the finite size exhibits a rotational motion due to the attractive tension by the Rabi coupling. If we consider the rotating frame co-moving with the domain wall, it is seen as a static configuration in this frame.

To see the stability of moving domain wall in a simple situation, we first consider the energetic stability of a moving domain wall with a constant velocity V along the x -direction. In the co-moving frame of the velocity V , the GP equation reads

$$i \frac{\partial \psi_j}{\partial t} = -\frac{\partial^2 \psi_j}{\partial x^2} - \tilde{\mu} \psi_j + |\psi_j|^2 \psi_j + \gamma |\psi_{\bar{j}}|^2 \psi_j - \omega_R \psi_{\bar{j}} + iV \frac{\partial \psi_j}{\partial x}. \quad (17)$$

Here, the velocity V is scaled by the sound velocity ξ/τ . Using Eq. (17), we analyze the energetic stability of the domain wall solution satisfying the boundary condition similar to Sec. III A through the imaginary time evolution. We show the stability boundary for $V = 0.2$ and $V = 0.4$ in Fig. 1; the stability region becomes narrower as V increases.

Next, we turn to the rotating frame with the frequency Ω_{prec} . When we suppose the domain wall along the y -axis and neglect the influence due to the vortices at the edge of the wall, we can approximately employ Eq. 17 with the y -dependent velocity $V = -\Omega_{\text{prec}} y$ to discuss the stability problem. The precession frequency of the vortex

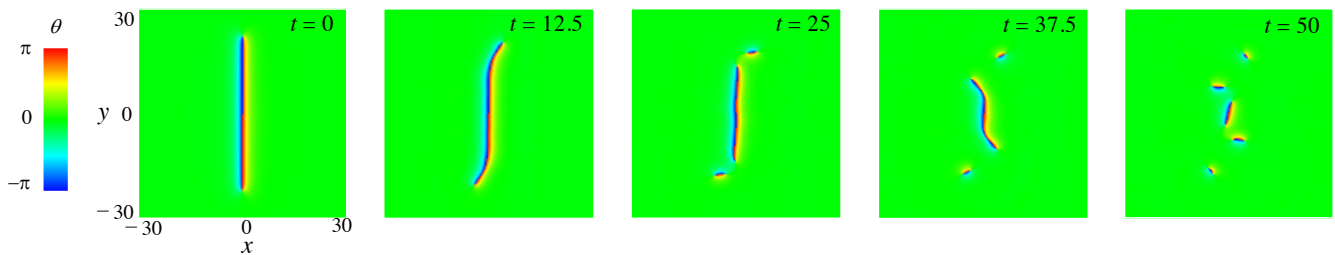


FIG. 6. The snapshot of the unstable dynamics of the domain wall of the relative phase for $L = 45$. The panels show the profile of the relative phase defined with the range $-\pi \leq \theta \leq \pi$. The parameters are $\gamma = 0$ and $\omega_R = 0.1$

molecule is approximately given by $\Omega_{\text{prec}} \simeq 8\sqrt{2\omega_R}/(\pi L)$ [14]. For $\omega_R = 0.1$ we find the velocity of the wall at the edge is $V_{\text{prec}} \sim 0.5$; the intermediate region of the wall precesses with the velocity below 0.5. Thus, when we take account of the rotational motion of the domain wall, the stability is significantly reduced for outer region away from the center of the wall. This behavior is clearly seen in Fig. 6, where the disintegration occurs first near the edges.

V. CONCLUSION

We study the transverse instability and disintegration dynamics of the domain wall of the relative phase in Rabi-coupled two-component BECs, motivated by the numerical observation in Refs. [14, 16]. Using the exact

solutions, we construct the phase diagram representing the stability of the domain wall. In the unstable regime, the domain wall exhibits dynamical instability associated with the transverse displacement, known as the snake instability. The instability causes the disintegration of the domain wall into the small pieces, namely the vortex molecules. The growth time and the size of the resulting vortex molecules are in fairly agreement with the prediction by the BdG analysis.

ACKNOWLEDGMENTS

The work of K.K. is supported by KAKENHI from the Japan Society for the Promotion of Science (JSPS) Grant-in-Aid for Scientific Research (KAKENHI Grant No. 18K03472).

-
- [1] Y. S. Kivshar and B. Luther-Davies, Dark optical solitons: physics and applications, *Physics reports* **298**, 81 (1998).
 - [2] L. Carr and J. Brand, *Multidimensional solitons: Theory, in Emergent Nonlinear Phenomena in Bose-Einstein Condensates* (Springer, 2008) pp. 133–156.
 - [3] A. E. Muryshev, H. B. van Linden van den Heuvell, and G. V. Shlyapnikov, Stability of standing matter waves in a trap, *Phys. Rev. A* **60**, R2665 (1999).
 - [4] J. Brand and W. P. Reinhardt, Solitonic vortices and the fundamental modes of the “snake instability”: Possibility of observation in the gaseous bose-einstein condensate, *Phys. Rev. A* **65**, 043612 (2002).
 - [5] D. L. Feder, M. S. Pindzola, L. A. Collins, B. I. Schneider, and C. W. Clark, Dark-soliton states of bose-einstein condensates in anisotropic traps, *Phys. Rev. A* **62**, 053606 (2000).
 - [6] B. P. Anderson, P. C. Haljan, C. A. Regal, D. L. Feder, L. A. Collins, C. W. Clark, and E. A. Cornell, Watching dark solitons decay into vortex rings in a bose-einstein condensate, *Phys. Rev. Lett.* **86**, 2926 (2001).
 - [7] P. Öhberg and L. Santos, Dark solitons in a two-component bose-einstein condensate, *Phys. Rev. Lett.* **86**, 2918 (2001).
 - [8] T. Busch and J. R. Anglin, Dark-bright solitons in inhomogeneous bose-einstein condensates, *Phys. Rev. Lett.* **87**, 010401 (2001).
 - [9] C. Becker, S. Stellmer, P. Soltan-Panahi, S. Dörscher, M. Baumert, E.-M. Richter, J. Kronjäger, K. Bongs, and K. Sengstock, Oscillations and interactions of dark and dark-bright solitons in bose-einstein condensates, *Nature Physics* **4**, 496 (2008).
 - [10] S. Coen and M. Haelterman, Domain wall solitons in binary mixtures of bose-einstein condensates, *Phys. Rev. Lett.* **87**, 140401 (2001).
 - [11] C. Qu, L. P. Pitaevskii, and S. Stringari, Magnetic solitons in a binary bose-einstein condensate, *Phys. Rev. Lett.* **116**, 160402 (2016).
 - [12] D. Son and M. A. Stephanov, Domain walls of relative phase in two-component bose-einstein condensates, *Physical Review A* **65**, 063621 (2002).
 - [13] K. Kasamatsu, M. Tsubota, and M. Ueda, Vortex molecules in coherently coupled two-component bose-einstein condensates, *Physical review letters* **93**, 250406 (2004).
 - [14] M. Tylutki, L. P. Pitaevskii, A. Recati, and S. Stringari, Confinement and precession of vortex pairs in coherently coupled bose-einstein condensates, *Physical Review A* **93**, 043623 (2016).
 - [15] L. Calderaro, A. L. Fetter, P. Massignan, and P. Wittek, Vortex dynamics in coherently coupled bose-einstein condensates, *Physical Review A* **95**, 023605 (2017).

- [16] M. Eto and M. Nitta, Confinement of half-quantized vortices in coherently coupled bose-einstein condensates: Simulating quark confinement in a qcd-like theory, *Physical Review A* **97**, 023613 (2018).
- [17] A. Usui and H. Takeuchi, Rabi-coupled countersuperflow in binary bose-einstein condensates, *Physical Review A* **91**, 063635 (2015).
- [18] D. Hall, M. Matthews, C. Wieman, and E. A. Cornell, Measurements of relative phase in two-component bose-einstein condensates, *Physical Review Letters* **81**, 1543 (1998).
- [19] M. Matthews, B. Anderson, P. Haljan, D. Hall, M. Holland, J. Williams, C. Wieman, and E. Cornell, Watching a superfluid untwist itself: Recurrence of rabi oscillations in a bose-einstein condensate, *Physical review letters* **83**, 3358 (1999).
- [20] E. Timmermans, Phase separation of bose-einstein condensates, *Physical review letters* **81**, 5718 (1998).
- [21] P. Ao and S. Chui, Binary bose-einstein condensate mixtures in weakly and strongly segregated phases, *Physical Review A* **58**, 4836 (1998).
- [22] S. K. Adhikari, Stability and collapse of a coupled bose-einstein condensate, *Physics Letters A* **281**, 265 (2001).
- [23] N. Dror, B. A. Malomed, and J. Zeng, Domain walls and vortices in linearly coupled systems, *Physical Review E* **84**, 046602 (2011).
- [24] M. Abad and A. Recati, A study of coherently coupled two-component bose-einstein condensates, *The European Physical Journal D* **67**, 148 (2013).
- [25] K. Kasamatsu, M. Tsubota, and M. Ueda, Spin textures in rotating two-component bose-einstein condensates, *Physical Review A* **71**, 043611 (2005).
- [26] K. Kasamatsu, M. Tsubota, and M. Ueda, Vortices in multicomponent bose-einstein condensates, *International Journal of Modern Physics B* **19**, 1835 (2005).
- [27] M. Eto and M. Nitta, Vortex trimer in three-component bose-einstein condensates, *Physical Review A* **85**, 053645 (2012).
- [28] M. Cipriani and M. Nitta, Crossover between integer and fractional vortex lattices in coherently coupled two-component bose-einstein condensates, *Physical review letters* **111**, 170401 (2013).
- [29] D. S. Dantas, A. R. Lima, A. Chaves, C. Almeida, G. Farias, and M. Milošević, Bound vortex states and exotic lattices in multicomponent bose-einstein condensates: The role of vortex-vortex interaction, *Physical Review A* **91**, 023630 (2015).
- [30] A. Aftalion and P. Mason, Rabi-coupled two-component bose-einstein condensates: Classification of the ground states, defects, and energy estimates, *Physical Review A* **94**, 023616 (2016).
- [31] B. M. Uraga and A. Lamacraft, Infinite lattices of vortex molecules in rabi-coupled condensates, *Physical Review A* **97**, 043609 (2018).
- [32] S.-H. Shinn and U. R. Fischer, Mesoscopics of half-quantum vortex pair deconfinement in a trapped spin-one condensate, *Physical Review A* **98**, 053602 (2018).
- [33] C. Qu, M. Tylutki, S. Stringari, and L. P. Pitaevskii, Magnetic solitons in rabi-coupled bose-einstein condensates, *Physical Review A* **95**, 033614 (2017).
- [34] H. Takeuchi, N. Suzuki, K. Kasamatsu, H. Saito, and M. Tsubota, Quantum kelvin-helmholtz instability in phase-separated two-component bose-einstein condensates, *Physical Review B* **81**, 094517 (2010).
- [35] N. Suzuki, H. Takeuchi, K. Kasamatsu, M. Tsubota, and H. Saito, Crossover between kelvin-helmholtz and counter-superflow instabilities in two-component bose-einstein condensates, *Physical Review A* **82**, 063604 (2010).
- [36] M. Eto, K. Kasamatsu, M. Nitta, H. Takeuchi, and M. Tsubota, Interaction of half-quantized vortices in two-component bose-einstein condensates, *Physical Review A* **83**, 063603 (2011).